Ocean Engineering xxx (xxxx) xxx

Contents lists available at ScienceDirect

Ocean Engineering

journal homepage: www.elsevier.com/locate/oceaneng

Experimental study on reduction of scouring and tsunami energy through a defense system consisting a seaward embankment followed by vertically double layered vegetation

Md Abedur Rahman [a], Norio Tanaka [a,b,*], Nijati Reheman [a]

[a] Graduate School of Science and Engineering, Saitama University, 255 Shimo-okubo, Sakura-ku, Saitama-shi, Saitama, 338-8570, Japan
[b] International Institute for Resilient Society, Saitama University, 255 Shimo-okubo, Sakura-ku, Saitama-shi, Saitama, 338-8570, Japan

ARTICLE INFO

Keywords:
Sea embankment
Tsunami overflow
Erosion
Scour
Coastal forest
Energy loss

ABSTRACT

To countermeasure the scouring and tsunami energy reduction, this study conducted a series of laboratory experiments where vertically double layered vegetation (VDLV) was introduced behind the seaward embankment on a gravel bed. The experimental results demonstrated that the overtopping flow from the embankment experienced a submerged hydraulic jump over the embankment, against all the considered cases. The dense VDLV i.e. dense ($G/d = 0.041$, where G is the clear gap between the cylinders in the cross-stream direction, and d is the cylinder diameter) short submerged vegetation (L_1) incorporated within a sparse ($G/d = 2.125$) tall emergent vegetation (L_2) influenced the scour phenomena. It reduced the relative scoured depth by approximately 29 – 41% at the embankment toe, the maximum scoured depth by approximately 29 – 37%, and the scoured length by approximately 28 – 34%, as compared to that of single embankment system. Furthermore, dense VDLV provided the maximum i.e. 49 – 53%, loss to the total flow energy. The increase in the density of L_1 in VDLV offered a larger drag to the flow by shifting the position of the submerged hydraulic jump more towards the embankment top; hence, consequently resulted in significant reduction of scoured depth, scoured length and energy of the tsunami flow.

1. Introduction

Following the Great East Japan Tsunami (GEJT) in 2011, a large-scale tsunami broke numerous coastal structures i.e. large embankments, tsunami gates, sea walls etc. (Tappin et al., 2012), and caused a fatal damage to the people lives (both socioeconomic and household properties) as well as the natural structures (Suppasri et al., 2012; Tanaka, 2012). Based on field surveys (Kato et al., 2012; Mikami et al., 2012; Tokida and Tanimoto 2014; Tanaka and Sato, 2015), many studies reported that, the possible mechanism of the seaward embankment failure was due to the local scouring on the ground. Since such a massive tsunami is likely to happen in the near future, the effective countermeasure against scouring caused by such tsunami is highly important. Many researches revealed (Afreen et al., 2015; Tanaka and Sato., 2015; Takegawa et al., 2017) and demonstrated (Noguchi et al., 1997; Bricker et al., 2012; Sassa et al., 2016; Takegawa et al., 2017) the scour process behind an embankment by experimental investigations, but the effective design procedure against scour countermeasure along with the reduction of tsunami flow is still limited.

For scour countermeasure, Motobe et al. (2014, 2016), and Yoshida et al. (2018) did laboratory experiments and concluded that, the placement of concrete blocks followed by seaward embankment can allow the overflowing water in stream-wise direction and shift the generation of scour hole further downstream from the embankment toe. Takegawa et al. (2019) conducted an experimental study for the scour countermeasures by putting a geogrid over a gravel bed (average particle diameter, $d_{50} = 3$ mm) starting from the toe of the embankment. They clarified that due to the influence of geogrid (mainly due to closer mesh size), scour holes moves away from the embankment; however, it is difficult to install geogrid along the coastal regions as vast areas are needed to be filled by gravel beds, and the land will be of no further use. If the scour hole moves further downstream of embankment, it would be dangerous to the downstream structures. Also, the countermeasure against scour by using concrete blocks requires the transportation of

* Corresponding author. Graduate School of Science and Engineering, Saitama University, Japan and International Institute for Resilient Society, Saitama University, 255 Shimo-okubo, Sakura-ku, Saitama-shi, Saitama, 338-8570, Japan.
E-mail address: tanaka01@mail.saitama-u.ac.jp (N. Tanaka).

https://doi.org/10.1016/j.oceaneng.2021.108816
Received 14 April 2020; Received in revised form 6 January 2021; Accepted 28 February 2021
0029-8018/© 2021 Elsevier Ltd. All rights reserved.

heavy construction materials, and massive excavation process will increase the construction cost which is not feasible based on the economic point of view. In present age, the significance of coastal vegetation (natural structures) as a function of tsunami mitigation has drawn much attention in the research field due to its multipurpose function such as energy loss, a smooth-landing location and debris trapping (Shuto, 1987). Moreover, vegetated foreshore can effectively reduce the wave loads on coastal dykes by offering resistance (Vuik et al., 2016). For the mitigation of tsunami energy, the coastal forest is being considered as an effective natural protection measure with respect to both environmental and economic aspects (Tanaka, 2009; Yanagisawa et al., 2010).

After a lesson learned from the GEJT, the mitigation strategy against tsunami inundation is drifting from only sea embankment to hybrid system arrangement of seaward levee and coastal vegetation. For instance, several studies investigated different types of mitigation systems against tsunamis such as Tanaka et al. (2006) examined the effect of coastal forest over a sand dune behind the seaward levee, Fadly and Murakami (2013) studied the combination of forest and moat, Zaha et al. (2019) investigated embankment with moat and vegetation. An investigation by Pasha and Tanaka (2017) showed that, the maximum energy reduction of tsunami current could be obtained by providing a dense forest with emergent condition, but in real scenario it could be difficult to implement a dense forest in the field. Tanaka et al. (2013) clarified that, a vertically double layered vegetation (VDLV), with the combination of *P. odoratissimus* and *Casuarina equisetifolia*, in Sri Lanka was found to be more efficient in tsunami mitigation. In addition, a post survey reported that, VDLV showed significant effectiveness in reducing the damage behind the forest in the 2004 Indian Ocean Tsunami (IOT) in Kalutara, Sri Lanka, 2005 (Tanaka et al., 2007). Some studies on investigating the effectiveness of VDLV have also been performed to countermeasure the disasters caused due to flood flows and tsunamis (e.g. Anjum and Tanaka, 2019a,b). Recently, Rashedunnabi and Tanaka (2019) experimentally clarified the mitigation effect of compound system with a combination of a coastal embankment followed by the coastal vegetation. The study showed that the different configurations of VDLV (short as submerged and tall as emergent) can effectively reduce the tsunami energy, increase the flow resistance compared to that of single layered vegetation (SLV) and could form different types of hydraulic jumps which further contributes in reduction of the tsunami energy. In addition, Anjum and Tanaka (2019c) experimentally investigated the effectiveness of discontinued VDLV, but there might be space limitation in the coastal regions. The previous studies have mainly focused on investigating the flow structures in the hybrid or compound defense structures under rigid bed conditions and they neglected scour phenomena, which is very important. However, there was no research on scour countermeasure behind a sea embankment with the introduction of VDLV against the tsunami flow on a gravel bed has been reported yet.

Thus, the main objectives of this study were to study the flow structures and to reduce the scouring behind an embankment with the introduction of VDLV in the downstream. To attain such objectives, laboratory tests were conducted with the arrangement of an embankment model (EM) followed by coastal vegetation model i.e. VDLV or SLV, over a gravel bed under the supercritical flow conditions. To justify the effectiveness of VDLV, at the back of EM, a vertically SLV was also considered. Three VDLV configurations were tested by varying porosity of the vegetation model (VM) against different hydraulic conditions.

2. Materials and methods

2.1. Experimental apparatus and procedures

Physical model experiments were performed in a glass sided flume channel with the dimensions of 5 m long, 0.7 m wide and 0.5 m deep (with a constant bed slope of 1/200), at Saitama University, Japan. The schematic diagram of model setup in the experimental flume is shown in Fig. 1i. The characteristics of tsunami flow and ground conditions implemented in this experimental study does not imply to any particular locations but were considered generally. In the GEJT, the Froude number ($Fr = V/(gh)^{0.5}$, where V is the depth averaged velocity (m/s), g is the gravitational acceleration (m/s^2), and h is the water depth (m)) in the coastal area was estimated about 1.5 in maximum by the moment of tsunami arrival near the coast of Misawa and Hachinohe regions in Japan (Nandasena et al., 2012). Also, Foytong et al. (2013), by video analysis, estimated that, the Froude number of flooding water depth varied from 1 to 1.5 in Iwaki and Kesennuma City in Japan. Therefore, taking those areas as a reference, to assure, model, and replicate the actual tsunami inundations, the flow conditions were attained in an empty channel. In model scale experiments, many studies also attained the flow conditions in an empty channel (Igarashi and Tanaka, 2016; Pasha and Tanaka, 2017; Rashedunnabi and Tanaka 2019; Anjum and Tanaka, 2019a). In addition, tsunami flow can be modeled by a pump-driven flow (Aniel-Quiroga et al., 2018). Thus, the targeted flow conditions were assured in the experimental runs. Since the tsunami flow was supercritical in coastal regions (Nandasena et al., 2012; Foytong et al., 2013); therefore, a downward facing slope has been selected in order to obtain supercritical flow conditions. Also, sometimes embankments were constructed on a sand dune, where the landward slope was downslope (Tanaka et al., 2013; Rashedunnabi and Tanaka, 2019; Rashedunnabi et al., 2019). The tsunami flood does not involve the wave crest and continues towards the inland regions with a prolonged time. Hence, the representation of tsunami inundation can be investigated by a quasi-steady flow (Nandasena et al., 2012; Ali et al., 2014; Igarashi and Tanaka, 2016; Rahman et al., 2020). Therefore, considering the supercritical and steady inland flow, Froude number similarity has been employed to decide the flow conditions representing the actual tsunami inundation. In this experiments, four initial Froude numbers ($Fr = V_o/(gh_o)^{0.5}$, where V_o is the depth averaged velocity (m/s), g is the gravitational acceleration (m/s^2), and h_o is the initial water depth (m)) of 1.28, 1.33, 1.38, and 1.44 were selected under the supercritical flow conditions. To select the initial flow conditions i.e., initial water depths (h_o) and initial Froude numbers (Fr), the discharges have been selected by the flow meter of the channel (Signet 8150 Flow Totalizer). Against every discharge, the water depth was measured along the center of the channel by a roller mounted point gauge depending on the variation of the water surface with an interval of 2 cm–10 cm. Therefore, four average initial water depths and the initial Froude numbers were selected corresponding to each known discharge. The depth averaged velocity was calculated by utilizing the continuity equation, $V = Q/(hb)$, (where Q is the discharge (m^3/s), h is the water depth (m) and b is the flume width (m)) against the known discharge. After installing the EM, the initial Froude numbers resulted in the overflowing water depths of 2.32, 2.9, 3.77, and 4.93 cm, respectively at the crest of the EM. For the bed materials as a soil layer, gravel particle with a median grain size (d_{50}) of 4.47 mm and dry density (ρ_s) of 2650 kg/m^3 was selected. Due to the higher threshold value for scouring by the cohesive soil material as a bed, the local souring occurred around the coastal dikes, and trees, at clear water condition in GEJT (Bricker et al., 2012; Ali and Tanaka, 2020). Many researchers have performed the laboratory investigations under clear water sour conditions by taking grain size of 4.5 mm as bed material for the soil layer, to attain the maximum scouring (Lenzi and Comiti 2003; Pagliara 2007; Afreen et al., 2015; Ali and Tanaka, 2020). Therefore, the grain size of the bed material has been selected to maintain the scouring at clear water condition for which the similarity law is not applicable. The gravel bed was placed starting from the toe of the EM to the further downstream with an area of 4 m in length, 0.7 m wide, and 0.23 m deep. A wooden flat plate having the same depth of soil layer was placed at the end of the channel as a support to prevent the washout of the soil layer during the flow. From the backend of the VM, the distance of the flat plate was kept approximately 3.25 m, in which the data was taken up to 2 m from the backend of the VM and a sufficient distance in the downstream region i.e. approximately 1.25 m, was also

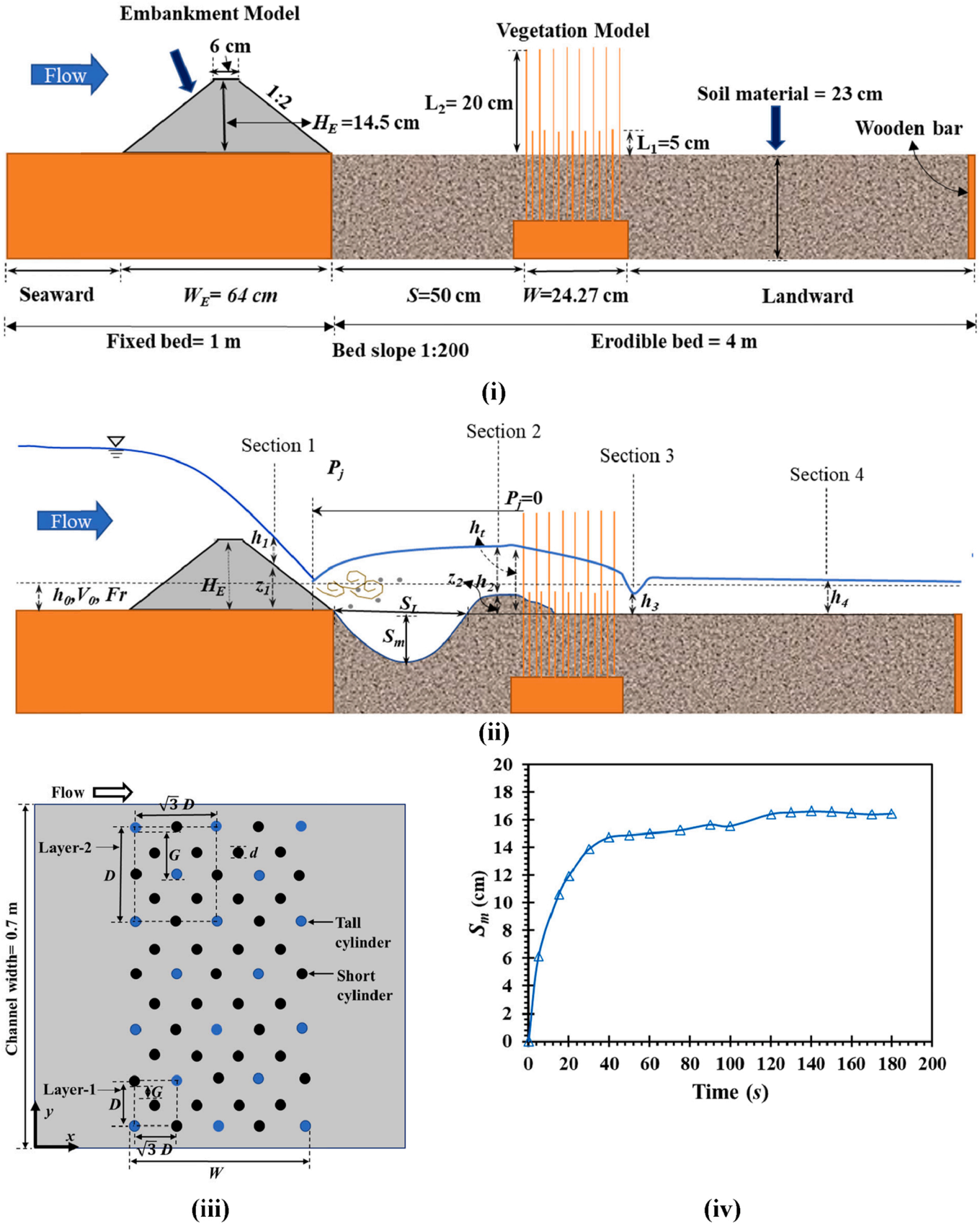


Fig. 1. i Experimental setup, **ii** Model schematic diagram and definition of different parameters, **iii** top view of model showing vegetation configuration, **iv** scour development against *Fr* 1.44 in Case 1.

made available (ignored for measurement) to eliminate the influence of the flat wooden plate at the end of flume channel. The scouring phenomena depends much on the characteristic of soil bed layer (i.e. cohesive, and non-cohesive material) in terms of water-soil bed interaction. Since it is very difficult to use cohesive material as a soil layer in model scale experiments, many researchers adopted non-cohesive particles as a soil layer in context of scouring study (Mitobe et al., 2014, 2016; Yoshida et al., 2018; Takegawa et al., 2019; Ali and Tanaka, 2020). However, the selection of particle size is an important factor when a non-cohesive particle is being used as a soil layer. Another important factor is the scour development for a specific particle size. The maximum scouring for a specific non-cohesive particle can be obtained when the scouring reaches an equilibrium condition (Takegawa et al., 2019; Ali and Tanaka, 2020). Due to this reason, the overflow duration in this study has been selected when the scoured depths reached the equilibrium stage. The development of scouring (S_m, maximum scoured depth) with respect to the overflow duration (in seconds) for Case 1 of $Fr = 1.44$, during the trial experiment is presented in Fig.1iv. It can be clearly seen that the equilibrium scoured depth can be achieved after the overflow duration (from EM) was around 160 s (2 min 40 s). In the actual physical scale of 1/100, it was around 1600 s, considering the Froude similarity law of physical scale. The duration of overflowing water can be occurred in an actual tsunami, so the equilibrium state should be reproduced in the study. Since the objective of this study was to reduce the maximum scouring with the introduction of VDLV, this overflow duration was selected after doing several trial cases to obtain the maximum scouring. In the trial cases, no significant variation of the scour profile was confirmed after this overflow duration (Fig. 1iv).

The whole experiment during the flow duration was recorded with HD (High-Definition) video camera (Olympus TG-835, with a frame rate of 1/30). The elevation of the water surface was measured by video analysis because the flow structures were very complex within the defense system, and oscillation of the water surface and duration of the experiment was small. The minimum and maximum depths were measured in multiple consecutive frames at a fixed point upon the variations in water surface and subsequently averaged. However, since the total duration of the experiment was small, only the water depth at section 1, section 2, section 3, and section 4 (Fig. 1ii) was measured with two roller mounted point gauges along the center of the channel operated by two persons. After completion of the experiments, the scour properties of the gravel bed were measured with a one-dimensional laser displacement meter (KEYENCE LK-500). The measurement interval of the data is 1.5–5 cm based on the variations of the gravel bed in both the cross-sectional and the longitudinal directions.

2.2. Model design and conditions of vegetation model (VM)

In this flume experiments, a physical model scale of 1/100 was selected for the experimental models. After the GEJT, an innovative coastal dyke system has been planned alongside the coast of Fukushima, Miyagi, and Iwate Prefectures in Japan including increasing the height and/or reconstruction of coastal dykes (Strusinska, 2017), where the proposed height of coastal dykes in Koizumi in Miyagi Prefecture is around 14.5 m. For this instance, the embankment height was scaled down to 14.5 cm height, 64 cm width, and side slope of 1:2, representing an embankment height of 14.5 m in the Fukushima, Miyagi, and Iwate Prefectures in Japan (Rashedunnabi and Tanaka, 2019; Rahman et al., 2020). In coastal areas, the seaward embankment are generally made of concrete and/or protected by concrete (Igarashi and Tanaka, 2016; Rashedunnabi and Tanaka, 2019; Rahman et al., 2020). Sometimes to prevent seepage, a short pile sheet was provided at the toe of the embankment. Thus, in context of the scouring studies followed by Afreen et al. (2015) and Takegawa et al. (2019), the foundation of the embankment was considered as fixed and EM was placed above the fixed bed and the seepage phenomena beneath the EM was ignored. However, if the EM would have been placed over a soil layer, both the scour and the flow phenomena may be slightly different compared with the results obtained in this study. Since the foundation of the EM was considered as fixed bed, which is an impermeable soil solid plate, the associated effects were ignored. Further studies can be however considered to clarify this effect by making the foundation of the EM as a soil layer. As for the VMs, the Japanese Pine tree, with median height of 15 m and diameter of 40 cm was available in Sendai Plain, Japan (Tanaka, 2012), was taken as a reference tree. Referring to the previous study (Iimura and Tanaka, 2012; Pasha et al., 2017), the trees were modeled by wooden cylinders having diameter (d) of 0.4 cm. The cylinders in VMs were designed in a staggered arrangement. In the GEJT, the trees having diameter larger than 0.4 m, were found unbroken (Tanaka et al., 2014) and during the 2004 IOT, the trees having diameter more than 0.3 m were also observed to be unbroken. Therefore, the tall cylinders (L_2) in both SLV and VDLV were modeled as circular wooden cylinders with a diameter of 0.4 cm and height of 20 cm. In VDLV the short cylinder with a height of 5 cm was taken as submerged vegetation (L_1). *Pandanus odoratissimus* (in tropical region) and *Pittosporum tobira* (in temperate region) trees grow with dense areal roots and a complex structure that offers a significant moment of the drag force (Tanaka et al., 2007). Both trees are representative trees in the coastal areas (Tanaka et al., 2007). In real situation, when tsunami inundation appears less than 5 m high *P. odoratissimus* was found to be more effective (Tanaka et al., 2007; Thuy et al., 2018). Therefore, the height of L_1 in all VDLV was taken as 5 cm from the ground level (considering 5 m in real scale). For enhancing the potentiality of the defense system as scour countermeasure along with tsunami mitigation, in this experiment three vertically double layer VMs was constructed on a wooden plate by inserting a short layer (L_1) within a sparse tall layer (L_2) and was arranged in a staggered arrangement. The layers in VDLV models were divided by varying the porosity (Pr) of VM. The porosities of L_1 were 0.78 (dense), 0.91 (intermediate), and 0.95 (partially intermediate), whereas the porosity of L_2 was fixed i.e. 0.98. The porosity of L_2 in SLV was also kept constant i.e. 0.98.

The models were constructed with long cylinders so that the bed materials can be inserted easily. The density of each models was represented by G/d value (where, G = clear gap between the cylinders in cross-stream direction, d = diameter of cylinder). The details of VMs configurations is presented in Fig. 1iii and Table 1. Four different VMs were considered i.e. SLV and VLDV, and were designed by varying condition of porosity, density and thickness of VMs. These models were installed within the gravel bed in the experimental flume covering the full width of the flume (as shown Fig. 1i). The width of vegetation (W) in stream-wise direction, can be represented by vegetation thickness: dn, which is a function of cumulative breast height diameter of the trees and is described as a function of the tree diameter at breast height and the number of trees (n) per unit area (m^2) in a rectangle with a frontal unit length along the coast and depth equal to the forest width (W) (Pasha and Tanaka, 2017). Referring to Shutto (1987), the value of dn in model scale was estimated as follows:

$$dn = \frac{2}{\sqrt{3}D^2} Wd \tag{1}$$

where the ratio $2/\sqrt{3}D^2$ means the density of the cylinder, and 2 means the cylinder numbers included inside a rectangular area under staggered system of arrangement (Fig. 1iii), W is the width of the forest, D is the distance among the cylinders in transverse direction, respectively (Fig. 1iii).

And, the porosity (Pr) of VM is calculated by following (Iimura and Tanaka, 2012):

$$Pr = 1 - \frac{n_t \pi d^2}{4} \tag{2}$$

where n_t is the density of vegetation.

Based on field surveys, Matsuba et al. (2014) and Tanaka and Sato

Table 1
Experimental conditions and vegetation configuration.

Case No.	Case	Initial water depth (cm)	Initial Froude No. "*Fr*"	Forest type	*D* (cm)	*d (cm)*	*G/d*	Porosity "*Pr*" (%)	Vegetation thickness *"dn"* (No. cm)	*W* (cm)
1	OE	2.22, 2.82, 3.3, 4.5	1.28, 1.33, 1.38, 1.44	–	–	–	–	–	–	–
2	ESLV	2.22, 2.82, 3.3, 4.5	1.28, 1.33, 1.38, 1.44	Sparse-L_2 only	2.5	0.4	2.125	98	179.36	24.27
3	$EVDLV_{L1_95}$	2.22, 2.82, 3.3, 4.5	1.28, 1.33, 1.38, 1.44	Inter-L_1	1.67	0.4	1.083	95	180.58	24.27
				Sparse-L_2	2.5	0.4	2.125	98	179.36	24.27
4	$EVDLV_{L1_91}$	2.22, 2.82, 3.3, 4.5	1.28, 1.33, 1.38, 1.44	Inter-L_1	1.25	0.4	0.563	91	717.43	24.27
				Sparse-L_2	2.5	0.4	2.125	98	179.36	24.27
5	$EVDLV_{L1_78}$	2.22, 2.82, 3.3, 4.5	1.28, 1.33, 1.38, 1.44	Dense-L_1	0.833	0.4	0.041	78	1615.51	24.27
				Sparse-L_2	2.5	0.4	2.125	98	179.36	24.27

Note: OE: only embankment; ESLV: embankment followed by SLV model; EVDLV: embankment followed VDLV model (L_1+L_2; L_1 = submerged vegetation layer, L_2 = emergent vegetation layer); the subscripts L1_95, L1_91, and L1_78 denotes the porosities of submerged layer i.e., 95%, 91%, and 78%, respectively.

(2015) reported that due to the overtopping of tsunami flow in the GEJT, severe erosion occurred, and scoured length were varied from 4 to 31.78 m. However, the scour properties i.e. scour length and depth, rose when the energy head and the force of the tsunami current increased (Tanaka and Sato, 2015). A study by Matsuba et al. (2014) observed that, the trees that were planted in close proximity to the levee on the landslide were displaced and generated a significant amount of floating debris. On the other hand, the coastal forest that has no gap in between the embankment and forest was entirely destroyed due to overtopping tsunami. For this instance, in the present study, a gap was kept as 0.5 m in between the EM and VMs, considering an effective measure as scour countermeasure and energy reduction of tsunami flow. Since, the embankments in the coastal regions were protected by concrete, so EM was considered as a fixed bed condition and was placed over the fixed bed in the flume channel at 1 m distance as of the inlet tank. Both the SLV and VDLVs were placed on a gravel bed downstream of the EM with a gap of 0.5 m. The VMs occupied almost full width of the flume channel while keeping a small space amongst the exterior vegetation cylinder and the flume wall. Several researches (JSFM, 1998; Rashedunnabi and Tanaka, 2019; Tang et al., 2019) showed that, to reduce the side wall influence on the water surface profiles, the ratio amongst the flume width and the diameter of cylinder should to be larger than 5. For this reason, this proportion was maintained to reduce the side wall effect.

2.3. Non-dimensional parameters used in this study

In this model scale experiment, the physical models of the prototypes were scaled down to reduced sizes (considering a model scale of 1/100) to represent the real phenomena under controlled conditions. The schematic diagram of the basic flow structure and associated important parameters are shown in Fig. 1ii and 1iii. The following non-dimensional groups were derived by adopting the Buckingham's pi theorem:

$$f\left[Pr, Fr, Fr_1, Fr_I, Fr_S, \frac{G}{d}, dn,\ P_j{}', P_S{}', \frac{h_t}{h_0}, \frac{\Delta E_t}{E_1},\ \frac{\Delta E_1}{E_1}, \frac{\Delta E_3}{h_3}\right] = 0$$

where, *Pr* is the porosity of the VM, *Fr* ($= V_o/(gh_o)^{0.5}$) is the initial Froude number, Fr_1 ($= V_1/(gh_1)^{0.5}$) is the approach (upstream of hydraulic jump) Froude number of jump, Fr_I ($= V_I/(gh_I)^{0.5}$) is the averaged Froude number within the defense system, Fr_S ($= V_S/(gh_S)^{0.5}$) is the averaged Froude number within the scour hole, *G* is the clear gap of every single cylinder in the cross-stream direction, *d* is the diameter of cylinder, P_j' (=P_j/S) is the non-dimensional position of hydraulic jump on the downstream face of the EM, P_j is the position of the hydraulic jump on the downward face of the EM, *S* is the space in between the EM and the VMs, P_S' (=P_S/H_E), P_S is the position of the maximum scoured depth, H_E is the EM height, h_t is the elevation of tail water, ΔE_1 is the total energy loss through the system i.e., downstream of the VM, ΔE_1 is the energy loss due to hydraulic jump within the defense system, ΔE_3 is the energy loss due to hydraulic jump behind the VMs, E_1 is the specific energy at section 1.

For a better understanding, the defined non-dimensional parameters used in this study were further divided into two groups i.e. group 1 (non-dimensional parameters which can be manually controlled) and group 2 (uncontrolled non-dimensional parameters based on the experimental results). Thus, group 1 includes *Pr*, *Fr*, *G/d*, *dn*, and group 2 includes Fr_1, Fr_I, Fr_S, $P_j{}'$, $P_S{}'$, $\frac{h_t}{h_0}$, $\frac{\Delta E_t}{E_1}$, $\frac{\Delta E_1}{E_1}$, $\frac{\Delta E_3}{h_3}$.

2.4. Energy loss

To evaluate the effectiveness of the defense system as a function of mitigation from the effect of tsunami, the energy head was estimated based on the following equation (Chow, 1959):

$$E = z + y + \alpha\frac{V^2}{2g} \tag{4}$$

where *E* is the specific energy, *z* is the elevation of the bottom, *y* is the water depth, V is the depth averaged velocity, and α is the co-efficient for calculating the variations in velocity. In this study, the value of α is considered as 1 for SLV whereas it is taken as 1.1 for VDLVs (Anjum and Tanaka, 2019c). Since a hydraulic jump was formed in the gap between the EM and VMs, as well as the downstream of the VMs; thus, the energy loss was subdivided as:

i. Total energy loss ($\Delta E_t = E_1 - E_4$) due to the defense system (downstream of VM), and
ii. Energy loss due to hydraulic jump inside the defense system ($\Delta E_1 = E_1 - E_2$) and energy loss due to the formation of hydraulic jump downstream of VMs ($\Delta E_1 = (h_4 - h_3)^3/4(h_4h_3)$), where E_1, E_2, E_3, and E_4 is the specific energy at section-1 (in front of jump), section-2 (downstream of jump), section-3 (in the undular jumps downstream of VM) and section-4 (downstream of the VM), respectively.

3. Results

3.1. Submerged hydraulic jump and its characteristics

Fig. 2 shows the resulting water surface profiles against the varying condition of initial Froude number (*Fr*), after the placement of models in the flume. The representative photos of the scour and water surface profiles are presented in Fig. 3. Within the defense system, the overtopping flow experienced a submerged hydraulic jump over the downface of the EM slope for all the cases against the considered initial Froude numbers. The non-dimensional position (P_j' = P_j/S) of the submerged hydraulic jump toe on the downface slope of the EM is shown in Fig. 4i. Two different P_j' (<1, and >1) are described in this study, where $P_j' < 1$ denotes that the jump starts in between the EM toe and VM, and $P_j' > 1$

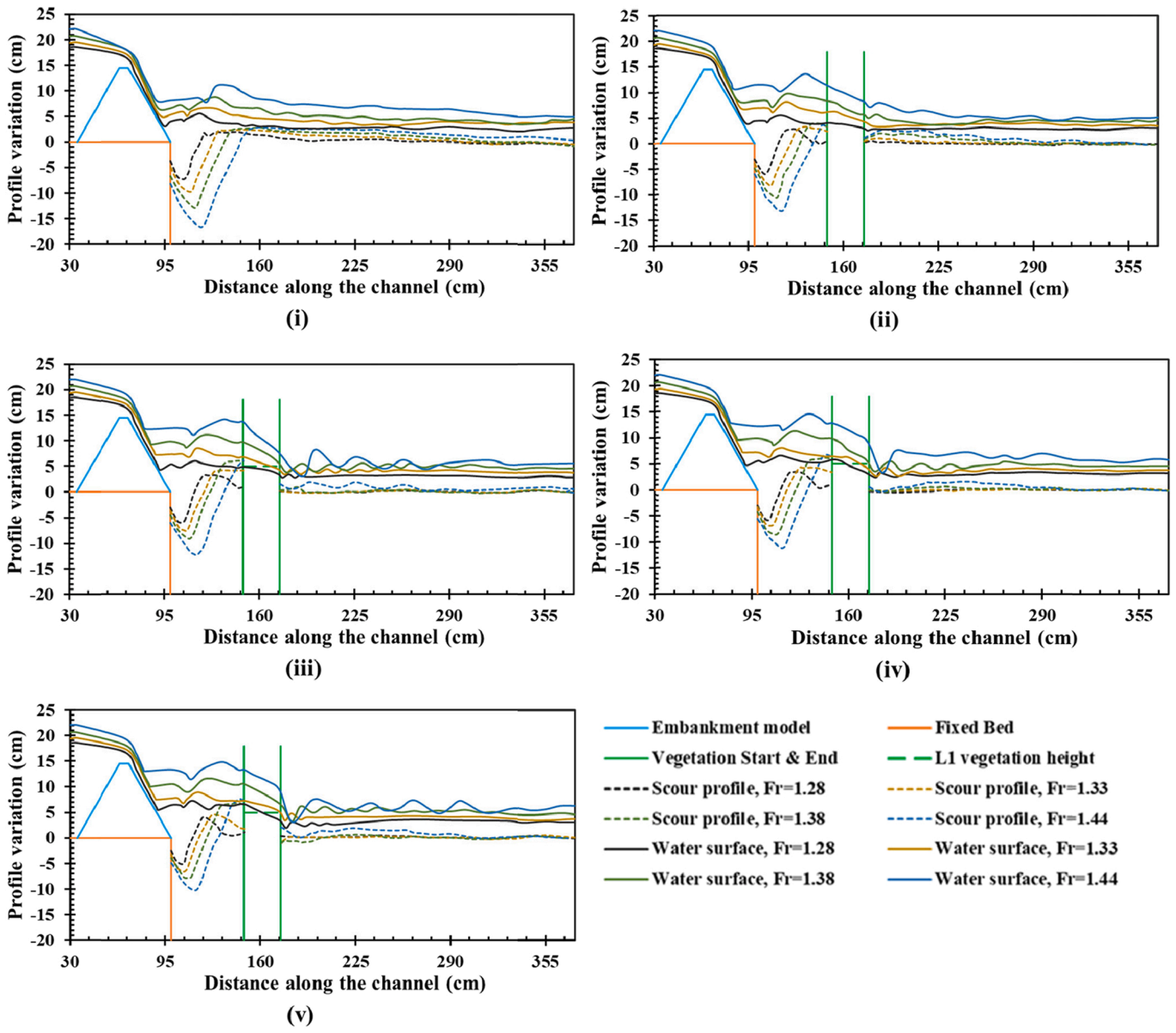


Fig. 2. Flow structure and scour profile around defense system against varying condition of initial Froude number "*Fr*", **i** Case 1, **ii** Case 2, **iii** Case 3, **iv** Case 4, **v** Case 5.

denotes that the jump starts on the downface of the EM. It can be clearly seen that, in all considered cases, the starting position of the submerged hydraulic jump lies on the downface of the EM slope i.e. $P_j' > 1$. In Case 1, the P_j' was much closer to the EM toe; however, when the VMs of different configuration were installed followed by an EM, the P_j' moved towards the EM top upon increasing the *Fr*. For the lowest *Fr* of 1.28 the P_j' was much closer to the EM toe but with the further increment of *Fr* the P_j' moved towards the EM top in all the cases. A gradually increasing trend of P_j' was observed in all the cases; however, the maximum value of P_j' was witnessed for Case 5 (i.e. when a dense VDLV was placed on the gravel bed behind an EM), whereas minimum values of P_j' were observed for Case 1. For the Case 4 and Case 5 these results are consistent with Rashedunnabi and Tanaka (2019). As the value of P_j' increased, the approach Froude number (Fr_1) decreased because of gradually varied flow on the downface of EM and consequently resulted in a comparatively higher relative elevation of tail water (h_t/h_0). Thus, a sharp decreasing trend of Fr_1 was observed for all the considered cases (Fig. 4ii). In comparison to that of SLV, a comparatively higher h_t/h_0 was observed in all the VDLV cases (Fig. 4iii).

3.2. Variation of scour profile

3.2.1. Variation of scour profile inside the defense system

In all the cases, scour starts from the toe of the EM and progresses further downstream (as shown in Figs. 2 and 5) which ultimately resulted a significant scour hole. The scoured depth increased gradually, and after reaching the maximum scoured depth, it decreased to the deposition level in all the considered cases. For the *Fr* 1.38 to 1.44 the level of deposition of soil particles was greater than the height of L_1 in Cases 3 to Case 5 (Fig. 5 c,d,e and Fig. 2 iii,iv,v); whereas, in Case 2 a comparatively lower deposition of soil particles was observed. However, the deposition of soil particles reached to ground level about 10 cm just in front of the VM in Cases 2 to 5 when *Fr* was 1.28 (Fig. 5 b,c,d,e and Fig. 2). A variation in resulted scour phenomena within the defense system in the cross-stream direction of the flume was observed in all the considered cases against different *Fr* conditions (Fig. 5). The scour profiles and the scour hole were large in Case 1 against all *Fr*. Similar scour profiles were observed by Takegawa et al. (2019), for Case 1. The magnitudes of scour profiles were significantly affected upon varying

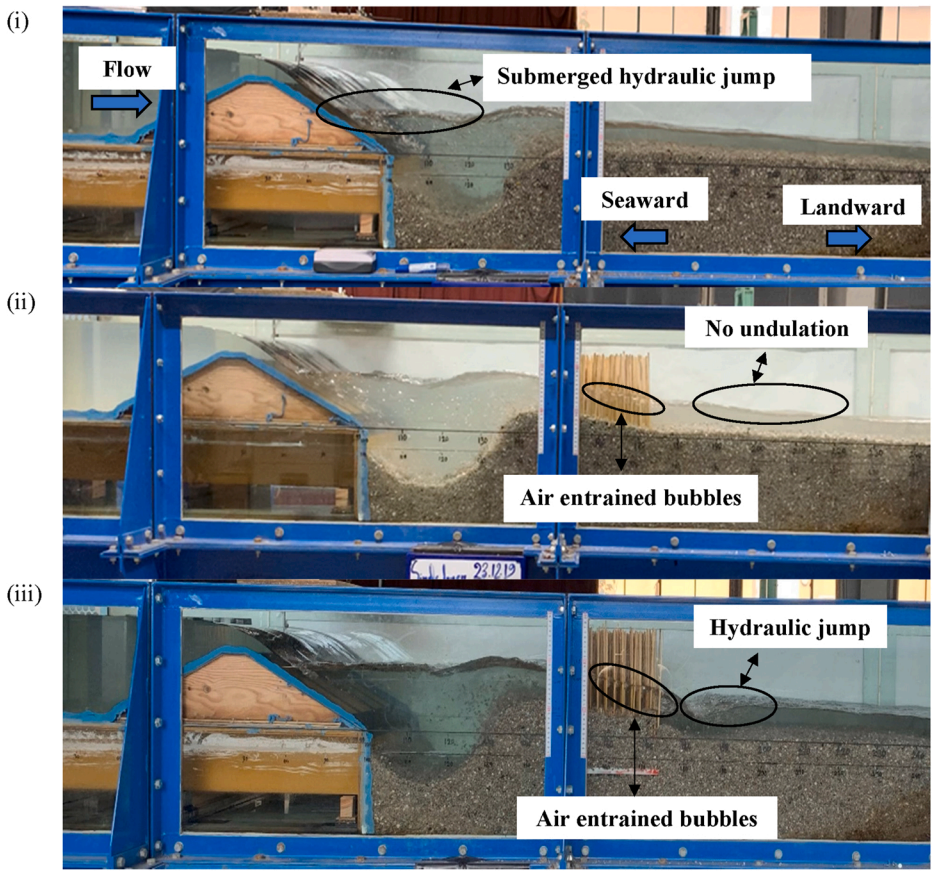


Fig. 3. Flow structure and scour profile around defense system for *Fr* of 1.44, **i** only embankment system (Case 1), **iii** with vertically single layer arrangement (Case 2), **iii** with vertically double layer dense arrangement (Case 5).

the different configurations of VM, and the VDLV cases reduced more scour compared to that of SLV case. In addition, a noticeable scour reduction is recognized in intermediate VDLV (Case 4, G/d = 0.563 for L_1, and G/d = 2.125 for L_2) and dense VDLV (Case 5, G/d = 0.041 for L_1, and G/d = 2.125 for L_2). In Case 5, it can be clearly witnessed that the scour hole at every *Fr* is significantly smaller than that in Case 1.

3.2.2. Scour and/or deposition phenomena at the downstream of VM

Fig. 6 illustrates the contour plots of the scour and/or deposition phenomena in the downstream of the VMs. It can be clearly seen that the downstream region of VM was almost undisturbed and no significant scouring and/or deposition of soil particles was observed in all the considered cases when *Fr* was 1.28 and 1.33, despite of the fact that some changes in the soil bed was observed due to flow. The removed soil particles between the defense system were travelled with the flow and deposited in the downstream region of VM. For the *Fr* of 1.33 and 1.44, the travelled soil material was deposited in the downstream in Case 2 to 5. Just behind the SLV model, the deposition was lowest, and it increased to maximum to further downstream when *Fr* was 1.33 and 1.44 (Fig. 2ii and Fig. 6b i,ii). Whereas, in VDLV cases, the lowest point of the deposition in soil particles (scouring phenomenon) was observed just below the generated hydraulic jumps (Fig. 2c,d,e and Fig. 6c,d,e i & ii). In Case 3, when the *Fr* was 1.44, an undulation of the soil bed was witnessed (Fig. 2c and Fig. 6cii). Just beneath the generated hydraulic jump point for the Case 5, very small scouring was noticed when the *Fr* was 1.44.

3.3. Effect of VM in scour characteristics

3.3.1. Effect of the porosity of VM on scour characteristics within the defense system

With the introduction of VMs behind the EM as a scour countermeasure, the scoured region within defense system was influenced significantly. The comparison of scour characteristics is presented in Fig. 7. It can be clearly seen that the scour characteristics i.e. scoured depth and scoured length, were significantly reduced by the decrease in porosity of L_1. The characteristics of scour were lowest in dense VDLV (Pr = 0.78 for L_1, and Pr = 0.98 for L_2) as compared to that of the intermediate VLDV (Pr = 0.91 for L_1, and Pr = 0.98 for L_2), partially intermediate VDLV (Pr = 0.95 for L_1, and Pr = 0.98 for L_2) and SLV (Pr = 0.98 for L_2). This indicates that both the scoured depth and scour length could be significantly influenced with decrement in porosity of L_1. This implies that the construction of a submerged layer along with its porosity within an emergent sparse forest plays a significant role in reduced scouring within the defense system.

3.3.2. Effect of VM on scoured depth

The scoured depth is also significantly reduced because of the resistance offered by the VM, so the assessment in comparison with single EM is needed. Fig. 7 shows the comparison of scoured depth at the toe of the EM and the maximum scoured depth caused by the overtopping flow. A sharp increasing trend in both the scoured depth at the toe of the EM (S_t) and maximum scoured depth (S_m) caused by overtopping flow (as shown in Fig. 7iii and 7i) is observed for Case 1 with the increase in *Fr* from 1.28 to 1.44, whereas a gradually increasing trend with comparatively lower magnitudes is found for SLV and VDLV cases (i.e. Case 2 to Case 5). In reducing the scoured depth at toe of the EM and the maximum scour within the defense system, the VDLV cases

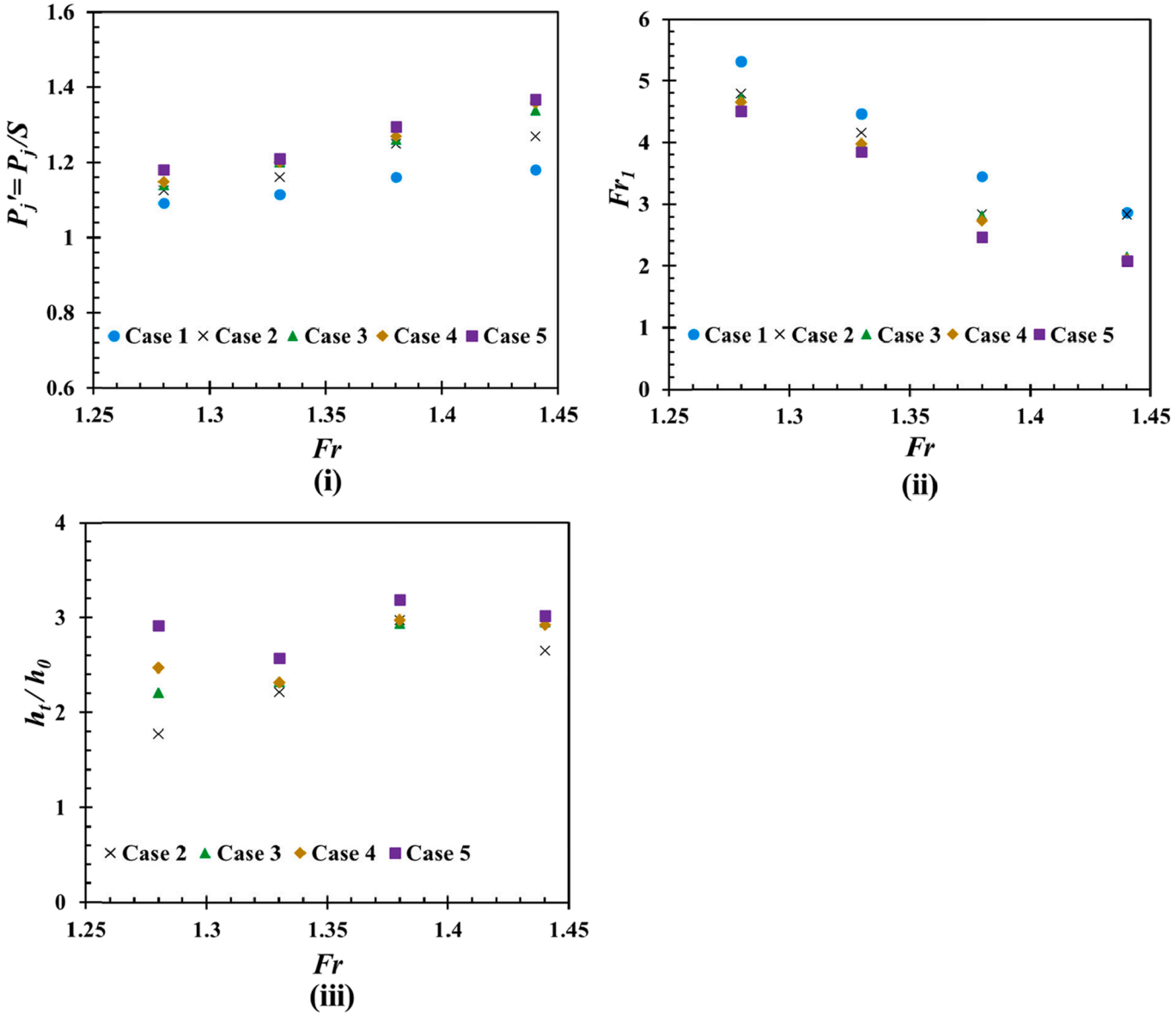


Fig. 4. Parameters related to submerged hydraulic jump against initial Froude number (*Fr*), **i** non-dimensional position of jump ($P_j' = P_j/S$), **ii** approach Froude number (in front of jump) of the jump (Fr_1), **iii** relative elevation of tail water (h_t/h_0).

performed better than SLV case, against the considered initial flow conditions. Among the VDLV cases, the dense VDLV (Case 5, G/d = 0.041 for L_1, and G/d = 2.125 for L_2) reduced more scour at the toe of the EM as well as within the defense system. The VDLV cases and sparse SLV (Case 2, G/d = 2.125 for L_2) reduced the toe scour approximately 12.2%–41% and 6.3%–26% (Table 3). In addition, the maximum reduction of S_t was found to be 29%–41% in Case 5 compared to that of Case 1, on the other hand Case 5 reduced the S_t approximately 15%–24% compared with the Case 2. The relative reduction of S_m for VDLV cases was found to be 17.1–37% (Table 4) compared to that of Case 1. On the contrary, SLV reduced S_m approximately by 7.2%–19.5%. The maximum S_m was found to be 10.18 cm, for Case 5, whereas it was 16 cm for Case 1 (Fig. 7i) when the *Fr* was 1.44. The relative maximum reduction of S_m for Case 5 varied from approximately 29%–37% (Table 4) against the considered *Fr* compared with the Case 1, whereas the corresponding variations were found to be 21%–23% compared to that of Case 2. In all the cases, a sharp increasing trend is witnessed for the non-dimensional position (P_S') of the maximum scoured depth (S_m) with the increase in *Fr* from 1.28 to 1.44 (Fig. 7ii). However, like S_t and S_m, the VDLV cases were effective enough in positioning the P_S'. In all the cases, with the increasing in *Fr*, the P_S' moved away from the toe of the EM but still lied in the center region which could ensure the safety of the defense structure. However, when there is no VM (i.e. Case 1), the P_S' moved further downstream compared to the vegetated conditions, which might destroy the structures downstream of it.

3.3.3. *Effect of VM on scoured length*

The relationship regarding the reduction in scoured length by the application of VM followed by an EM is shown in Fig. 7iv. In all the cases, a sharp increasing trend of scoured length (S_L) within the gap between the defense system is witnessed, against the varying condition of *Fr*. However, the magnitude was slightly reduced in Case 4 and Case 5. The SLV reduced the relative S_L around 9.7%–19.1% approximately (Table 5), whereas the corresponding variations were found to be approximately 18.3%–34% for the VDLV cases. The VDLV cases reduced the scoured length at about 6%–23% compared to that of SLV against the considered *Fr*. Among the three VDLV cases, the dense VDLV (i.e. Case 5), is witnessed to be more effective in reducing the scoured length

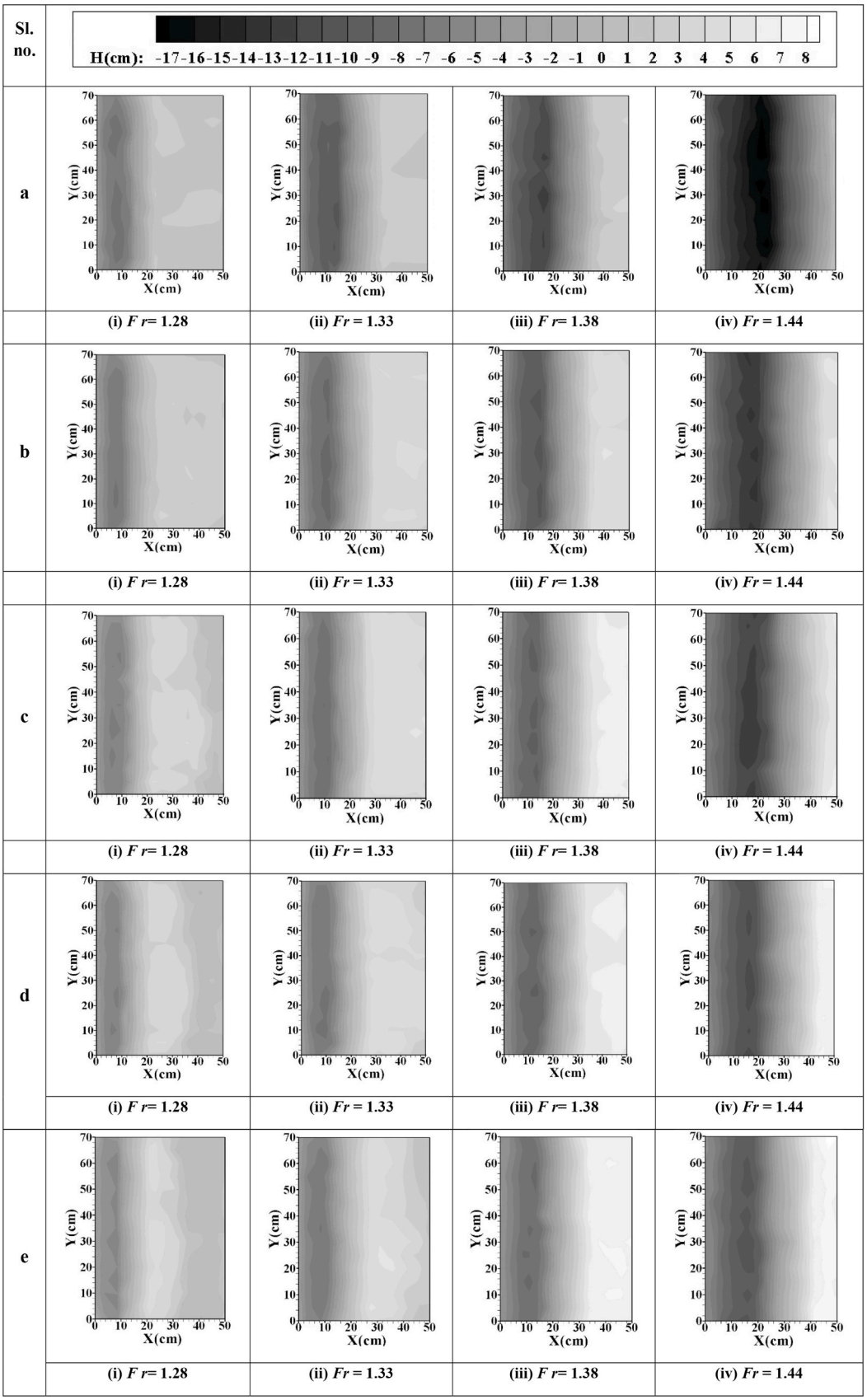


Fig. 5. Contour plot of the scour profile within the defense system against initial Froude number (*Fr*), **a** Case 1, **b** Case 2, **c** Case 3, **d** Case 4, **e** Case 5. Note: X-axis is the distance along the channel and Y-axis is the distance in the cross-stream direction of the channel, H-legend is the scoured/deposited depth.

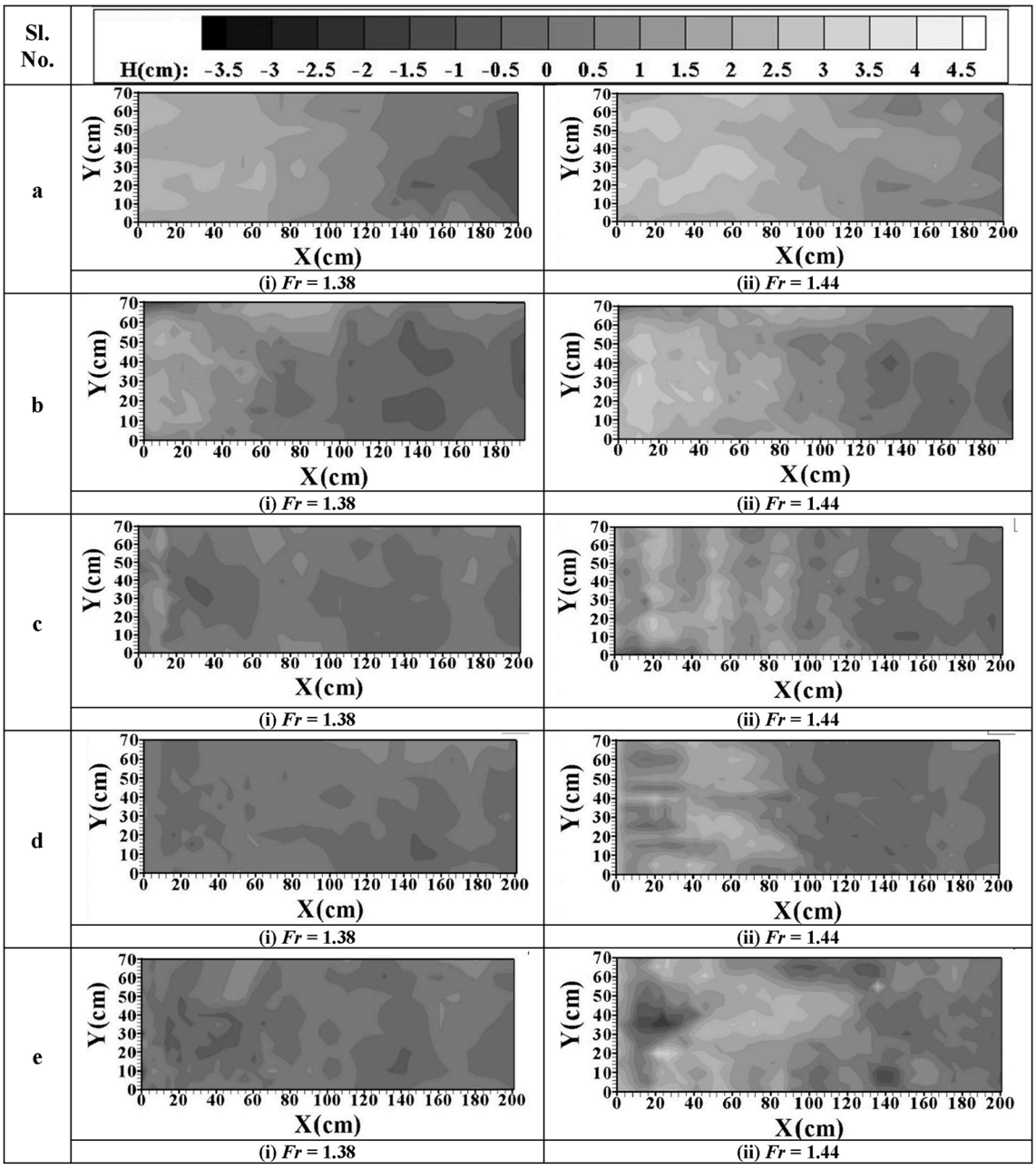


Fig. 6. Contour plot of the scour and/or deposition phenomena downstream of the vegetation model against initial Froude number (*Fr*), **a** Case 1, **b** Case 2, **c** Case 3, **d** Case 4, **e** Case 5. Note: X-axis is the distance along the channel and Y-axis is the distance in the cross-stream direction of the channel, H-legend is the scoured/deposited depth.

(Fig. 7iv). The maximum scoured length was found to be 32 cm for Case 5, whereas in Case 1, S_L was 48.2 cm when *Fr* was 1.44. The range of the maximum reduction obtained for Case 5 was about 28%–34% compared to that of Case 1, whereas the corresponding reduction was found to be 18%–21% compared to that of Case 2.

3.4. Energy loss

3.4.1. Effect of the density of VM on total energy loss

The density of the VM significantly affected the relative total energy loss. Fig. 8i indicates the difference of the relative total energy loss for each VM against varying condition of *Fr*. It can be clearly observed that, the relative total energy loss is maximum for dense VDLV i.e. Case 5 (G/d = 0.041 for L_1, and G/d = 2.125 for L_2) as compared to the intermediate VLDV i.e. Case 4 (G/d = 0.563 for L_1, and G/d = 2.125 for L_2), and partially intermediate i.e. Case 3 (G/d = 1.083 for L_1, and G/d = 2.125 for L_2) as well as sparse SLV (G/d = 2.125 for L_2 only). In addition, both intermediate and partially intermediate VDLV cases reduced more energy compared to that of sparse SLV. This implies that the introduction of a submerged shorter layer along with the variation in its porosity within an emergent sparse forest offered significant flow resistance and caused greater energy loss.

3.4.2. Energy loss through the defense system

The total energy reduction of the tsunami flow by the defense system ($\Delta E_t/E_1$) was defined in Eq. (4) and shown in Fig. 8i. The total energy loss consists of both the losses due to EM and VM along with the formation of hydraulic jumps downstream of VM. For all the considered cases, the relative total energy loss followed a gradually increasing trend when *Fr* increased from 1.28 to 1.38. But with the further increase in *Fr*

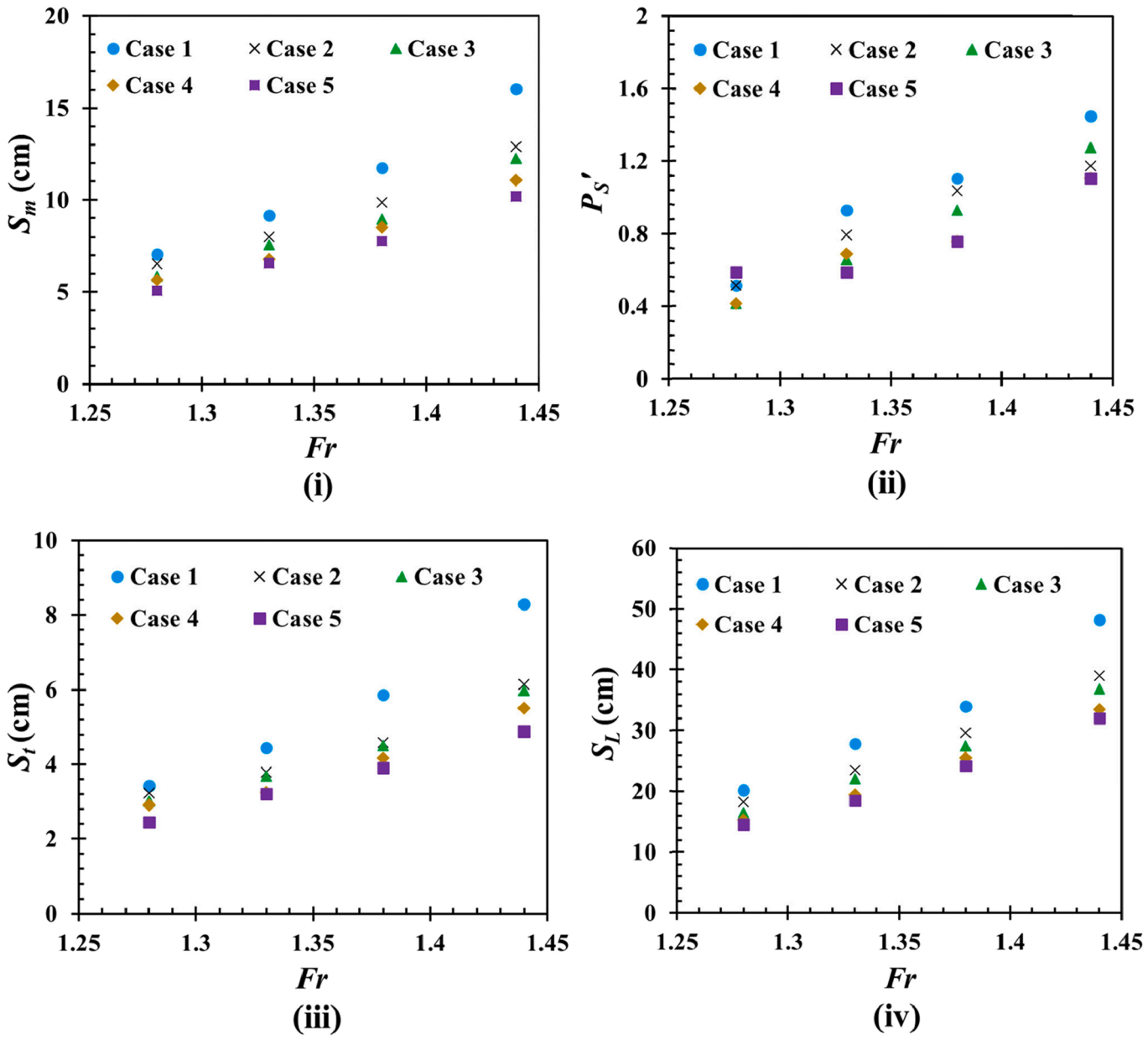


Fig. 7. Scour characteristics within the defense system against initial Froude number (*Fr*), **i** maximum scoured depth, **ii** non-dimensional position of maximum scour, **iii** scoured depth at toe of the embankment, **iv** scour length starting from embankment toe.

Table 2
Flow conditions within the defense system.

Fr	Fr_S					Fr_I			
	Case 1	Case 2	Case 3	Case 4	Case 5	Case 2	Case 3	Case 4	Case 5
1.28	0.150	0.154	0.160	0.171	0.164	0.561	0.545	0.420	0.404
1.33	0.132	0.141	0.135	0.155	0.155	0.430	0.550	0.602	0.427
1.38	0.134	0.153	0.175	0.198	0.218	0.311	0.463	0.505	0.512
1.44	0.177	0.180	0.189	0.231	0.283	0.287	0.295	0.427	0.425

Note: Fr_S is the average Froude number within the scour hole and Fr_I is the average Froude number in the gap (S) within the defense system.

from 1.38 to 1.44, the relative energy loss decreased gradually for Case 1 and Case 2, whereas a slightly decreasing trend was noted for the VDLV cases (Case 3 to Case 5). This outcome of gradually increasing and decreasing trend in relative total energy loss against *Fr* for VDLV is consistent with that witnessed in the experimental investigation of the flow through VDLV (Rashedunnabi and Tanaka, 2019), under the similar VM conditions (VM porosity and density). When SLV and VDLV were implemented at the back of an EM, the highest relative total energy loss was found to be around 12% and 26%, respectively, compared to that of Case 1 (OE case). In addition, the VDLV cases reduced further energy by approximately 20%–26% compared to that of Case 1. Nevertheless, the maximum relative total energy loss was found to be

Table 3
Comparison of relative reduction of S_t (in percentages) with respect to Case 1.

Initial Froude number, *Fr*	Case 2	Case 3	Case 4	Case 5
1.28	6.3	12.2	15.5	29
1.33	14.5	16.8	26.9	27.7
1.38	21.8	23	28.9	33.1
1.44	26	27.8	33.7	41

Table 4
Comparison of relative reduction of maximum scoured depth (in percentages) within the defense system with respect to Case 1.

Initial Froude number, *Fr*	Case 2	Case 3	Case 4	Case 5
1.28	7.2	17.1	19.8	29
1.33	12.6	17.3	26	28.3
1.38	15.8	23.8	27.3	33.8
1.44	19.5	23.5	31	37

Table 5
Comparison of relative reduction of scoured length (in percentages) within the defense system with respect to Case 1.

Initial Froude number, *Fr*	Case 2	Case 3	Case 4	Case 5
1.28	9.7	18.3	24.5	28
1.33	15.5	20.9	29.9	33.5
1.38	12.9	19.4	25.0	28.7
1.44	19.1	23.7	30.5	34

approximately 49%–53% for the dense VDLV case i.e. Case 5 (G/d = 0.041 for L_1, and G/d = 2.125 for L_2) with respect to the initial Froude number conditions.

3.4.3. Energy loss due to hydraulic jump

Since, the formation of hydraulic jump contributes to energy loss, hence the calculation of energy loss due to jump is important. The relative energy loss because of the formed hydraulic jump in the gap (S) ($\Delta E_1/E_1$) and the relationship of the relative loss of energy due to generation of the hydraulic jump behind the VMs ($\Delta E_3/h_3$) against *Fr* is shown in Fig. 8ii and 8iii. Within the defense system, the relative energy loss followed a sharp decreasing trend in Case 2 (i.e. SLV) (Fig. 8ii), for all the initial Froude number (*Fr*) conditions. However, when the *Fr* increased from 1.28 to 1.33, the energy reduction rate increased rapidly in Case 3 to 5 (i.e. VDLV cases), but with the further increasing in *Fr* from 1.33 to 1.44, the energy loss followed a sharp decreasing trend for Case 3 and a gradually decreasing trend for Case 4 and Case 5 (Fig. 8ii). The maximum value in energy loss was solely dependent on the relationship in between the higher value of P_j' and the inundation depth in the downstream of the VDLV Cases became inverse i.e. maximum and the minimum, respectively, because of the higher density and the lower porosity of L_1 in VM. The maximum relative energy loss is found to be around 35% in Case 2 for the lowest *Fr* of 1.28. However, when the *Fr* increased from 1.33 to 1.44 the VDLV cases reduced more energy compared to that of Case 2. For the highest *Fr* of 1.44, both Case 4 and 5 performs better by reducing the energy loss by more than 10% compared to that of Case 2. The proper hydraulic jumps were formed only with the VDLV cases (Case 3 to Case 5) when *Fr* ranged from 1.33 to 1.44 (Fig. 2iii, 2iv and 2v). A sharp decreasing trend was observed for Case 3 to Case 5, when *Fr* ranged from 1.33 to 1.38 (Fig. 8iii). But, with the further increase in *Fr* from 1.33 to 1.44, the relative energy loss follows an increasing trend in all VDLV cases (Fig. 8iii). This phenomena was occurred because the deposition of the bed materials was started behind VM for both *Fr* of 1.33 and 1.44 (Fig. 6c,d,e i & ii). However, dense VDLV case (Case 5) showed a comparatively higher percentage of relative energy reduction due to the generated hydraulic jump behind VM against the initial Froude number conditions. The loss of relative energy due to hydraulic jump in Case 5 contributed 13–19% to the total energy loss. Moreover, for the Case 2 and the lowest *Fr* of 1.28 for the Case 3 to 5, the energy loss could not be correctly calculated because of no proper formation of hydraulic jumps, rather than a small undulation of water surface and/or undular jump type phenomena was observed (Fig. 2).

4. Discussion

4.1. Flow and scour characteristics

This study examined the function of VM in fixed width condition as a scour countermeasure, as well as reduction of tsunami energy, and revealed the unique distribution of scour phenomena along with the interaction of an overtopping flow from the EM when a VDLV was implemented behind it. The overtopping flow generally approached to the downward slope of EM with a higher flow gradient which resulted in a higher velocity and Froude numbers, due to which the approach Froude numbers were high (Fig. 4ii), and significantly reduced the average Froude number in the scour hole (Fr_S) as well as within the defense system (Table 2). When this overtopping flow hits the ground, it causes a significant scouring which makes the defense structures vulnerable, as was found that the coastal embankments were severely destroyed in the GEJT (Tanaka and Sato, 2015; Jayaratne et al., 2016). Some of the previous research discussed that the counterclockwise roller vortex plays a significant role in the formation of increased scour hole (Bricker et al., 2012; Afreen et al., 2015; Takegawa et al., 2017). In the OE case i.e., Case 1, the roller vortex became large, and it increased the turbulence intensity, which consequently resulted a subcritical flow in the scour hole (Table 2). Due to the increased turbulence intensity, the shear stress also increased, which ultimately resulted in an increased scour hole. However, after installing the VM of different configurations behind the EM, the intensity of the roller vortex was reduced significantly because of shifting of the position of generated submerged hydraulic jump toward the embankment top. Thus, the Froude numbers in the scour hole were increased slightly in the VM cases compared to that of the OE case.

As a scour countermeasure at the embankment toe, experimental investigation by Mitobe et al. (2014, 2016) and Yoshida et al. (2018) recommended that implementation of concrete block behind a seaward embankment had allowed the direction of the overtopping water in streamwise direction and directed the production of scour hole away from the embankment. Takegawa et al. (2019) proposed that the placement of geogrid (with a mesh size of smaller than the average gravel particle diameter) over a gravel bed can reduce the magnitude of scouring that starts from the embankment toe. However, if the scour hole propagates to the further downstream then there is a significance chance that the downstream structures could be destroyed. Moreover, installation of large concrete blocks and placement of geogrid having size less than gravel particles is very difficult to implement in real fields and not feasible based on economic and environmental point of view, as these includes heavy construction process requiring massive amount of construction materials and manpower. These, literature gave us understanding about the implementation of a secondary structure as a countermeasure against the scouring and reduction of tsunami energy. Many recent studies indicated the significance of coastal forest as a function of tsunami mitigation (Tanaka et al., 2013; Pasha and Tanaka, 2017; Anjum and Tanaka, 2019c; Rashedunnabi and Tanaka, 2020). The problem regarding scouring could be solved by constructing a defense system by implementing VM behind a little remote position of a seaward EM. The scour profiles within the defense system i.e. in the gap region in between EM and VM, showed that the scouring could be significantly reduced when a VDLV and SLV were implemented behind an EM (Figs. 2 and 7). The dense VDLV reduced the scour characteristics i.e. scoured depths and length by offering a higher drag and reflection to the flow because of the reduced porosity in the short layer (*Pr* = 0.78 for L_1) as compared to the other VM cases (Fig. 7, Table 3, Tables 4 and 5). On the

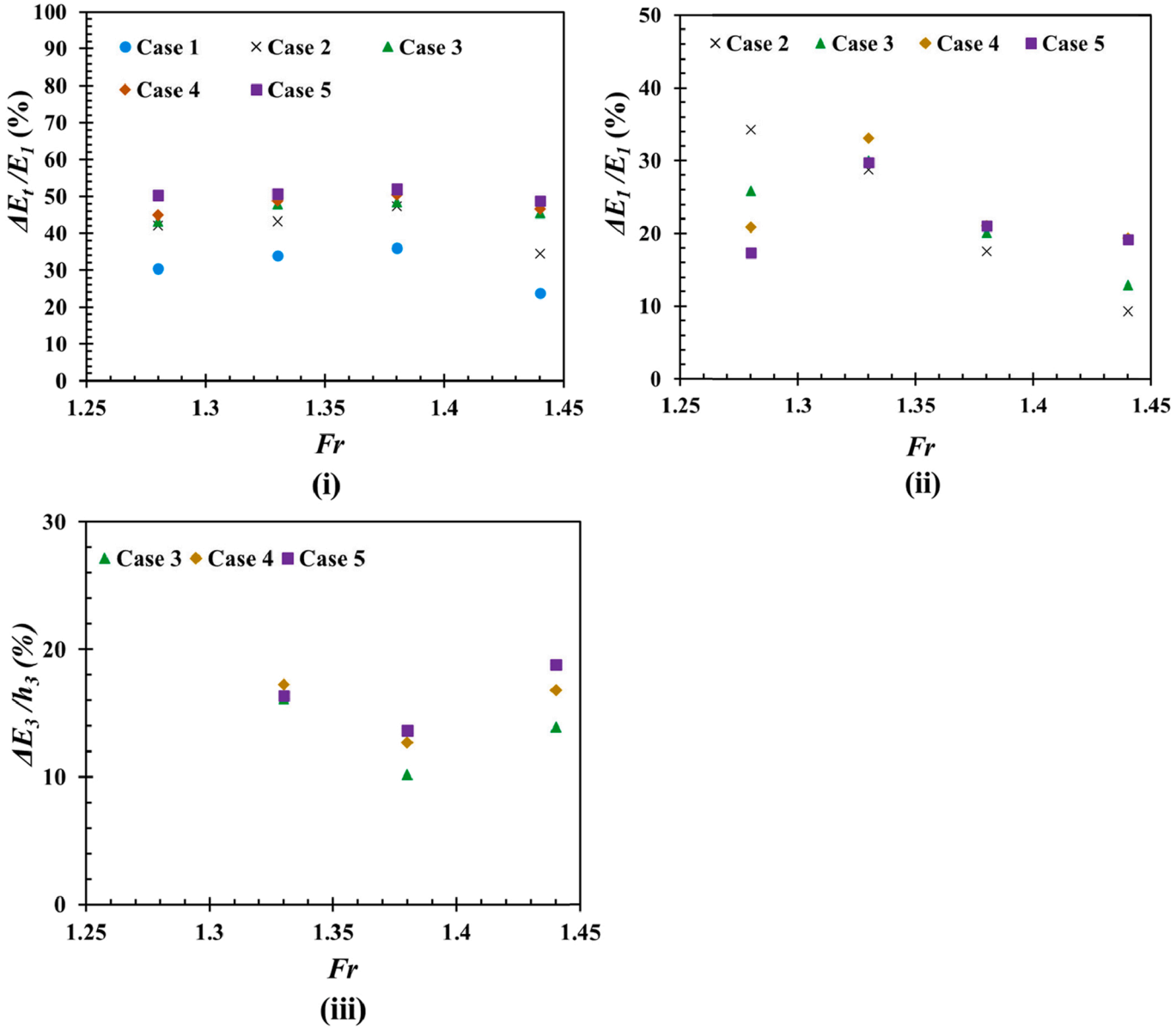


Fig. 8. Relative energy loss against initial Froude number for all the cases, **i** total relative energy loss ($\Delta E_t/E_1$, downstream of the vegetation model), **ii** relationship between relative energy loss due to hydraulic jump inside defense system ($\Delta E_1/E_1$), **iii** relationship between relative energy loss due to hydraulic jump ($\Delta E_3/h_3$) against initial Froude numbers.

other hand, because of high porosity ($Pr = 0.98$ for L_2) of SLV, it offered a lesser amount of resistance to the overtopping flow and resulted a more scouring compared to the VDLV. Hence, this phenomena i.e. decrement of porosity of VM, is in support for the protection of both defense structures in reducing the scouring phenomena.

The major reason of increased scour hole is the higher energy of the overtopping flow depth. With the increase in *Fr*, the overtopping flow depth increases, thus the increased scour holes was witnessed in all the considered cases. These results are consistent with the previous studies (Afreen et al., 2015; Tanaka and Sato, 2015; Takegawa et al., 2017). The elevated submerged jump toe on the upstream of EM results in a greater decline in the transverse velocity (Kawagoshi, 1990). Therefore, in a submerged jump, the near bed velocity alongside the flume becomes very low compared to that of the mean velocity. That is why when P_j' *of* the submerged hydraulic jump became larger, scouring was reduced significantly. In this study, when SLV and VDLV were placed followed by an EM as a secondary defense structure, the intensity of the submerged hydraulic jump was increased and also, water level inside the defense system was increased significantly (Fig. 2) due to the drag and resistance posed by the VMs. According to Chow (1959), these phenomena could be safest for the embankment structure since the coastal embankments are protected by concrete. In addition, an experimental investigation by Rashedunnabi and Tanaka (2019) had reported the same phenomena. The P_j' was greater when the porosity of L_1 in VDLV became low. Due to this reason, when a dense VDLV was placed behind an EM, the P_j' became larger i.e. the location of the submerged hydraulic jump toe shifted towards the toe of the EM top and elevation of tail water due to VMs became higher, because of low porosity in L_1 (Fig. 4i and 4iii) which consequently resulted less scouring within the gap between the defense system compared to that of OE and SLV. So, P_j' is found to be an important parameter to the flow structure which reduces the scouring significantly. Thus, controlling the P_j' is very important in reducing the magnitude of the scour hole.

Due to the significant erosion in Case 1, the increased scoured depth at the toe of the EM and the maximum scoured depth inside the defense system may result in a seepage failure at the toe of the EM due to the

removal of base soil layer. These phenomena can cause the foundation failure, bearing capacity failure, and can make the EM structure unstable (Sassa et al., 2016). However, due to the increased water cushion effect by the VM, the scouring was reduced and a maximum 41% reduction of scoured depth at the toe of EM was observed when a dense VDLV was placed behind the EM. An investigation by Sassa et al. (2016) discussed the tsunami overflow on seepage which may significantly affect the stability of the embankment. Due to the increased water cushion within the defense system, the VDLV models have reduced the scouring by causing less seepage due to suppressing the coupling effect of the overflow. Thus, decreasing the scouring phenomena within the defense system is safer for the stability of the EM.

4.2. Energy loss

Despite the fact that, the scour holes developing just behind the seaward embankments are considered to be the reason of breaching, these holes were reported to decrease the tsunami energy in the downstream region (Mitobe et al., 2016; Tanimoto and Tokida, 2012; Tanimoto et al., 2012). When a downstream structure is provided behind the seaward embankment, it can effectively reduce the fluid force (Radhedunnabi and Tanaka, 2020), moment index (Zaha et al., 2019), and momentum flux (Park et al., 2017), by posing resistance to the overtopping flow. These studies gave understanding that the energy loss can also be effectively reduced by implementing a VM behind a seaward EM. When VM was implemented, it reduced more energy compared to that of OE (Fig. 8i). An exponentially decreasing trend in energy loss was observed with increase in *Fr* from 1.38 to 1.44, for all the considered cases because the effect of energy loss by hitting the ground became relatively low with the rise of overtopping flow (Fig. 8i). The energy loss due to the hydraulic jump within the defense system is solely dependent on the jump characteristics (Rashedunnabi and Tanaka, 2019). Due to the drag and reflection offered by VMs, the elevation of tail water increased, and consequently P_j' was also increased (Fig. 4i and 4iii). As P_j' was increased, the scour hole was also reduced. Due to this, a slight decrement in energy loss due to jump was witnessed (Fig. 8ii) when porosity of L_1 was reduced. The same phenomena was observed by Rashedunnabi and Tanaka (2019). This study witnessed that the intensity of hydraulic jump behind VM was increased upon the increment of the density of VM along with the increment of *Fr*. In addition, the formed hydraulic jump contributed a significant amount of energy loss into the total relative energy loss in the VDLV cases (Fig. 8iii). However, the total energy loss was varied based on the larger P_j' value and the intensity of formed hydraulic jump just behind VMs. Thus, in the present study, P_j' is found to be an important parameter in reducing the total energy in the downstream of the VMs.

In this paper, it is witnessed that when a dense VDLV was implemented behind a seaward EM, it provided the satisfactory outcomes of maximum reduced scoured depth at the EM toe, maximum scoured depth within the defense system, scoured length as well as the overall energy loss, out of all the considered configurations. Therefore, as an effective design procedure against scour countermeasure and energy reduction of the tsunami flow, a landward dense VDLV ($G/d = 0.041$ for L_1, and $G/d = 2.125$ for L_2) could be implemented followed by a seaward EM i.e. Case 5. However, depending on the soil condition, if it becomes difficult to construct a dense VDLV along the coast, then in such case the intermediate VDLV ($G/d = 0.563$ for L_1, and $G/d = 2.125$ for L_2) could also be considered (i.e. Case 4).

5. Conclusion

In the present study, model scale flume experiments were conducted to investigate the effects of vegetation as a scour countermeasure as well as reduction of the tsunami energy behind a seaward embankment against supercritical flow conditions with a gravel bed. The conclusions derived from the current study are as follows:

- The overtopping flow from EM experienced a submerged hydraulic jump over the EM slope against all the initial Froude numbers (*Fr*) for all the considered model configurations. The flow caused significant scouring at the toe of EM due to direct collision with the ground, which initiated from the toe of EM and progressed towards downstream. However, the placement of the VMs behind an EM significantly influenced the intensity of the submerged hydraulic jump characteristics (position of jump, approach Froude number and tail water depth) within the defense system.
- The scoured depth within the defense system was significantly reduced with the introduction of VM behind the EM. The maximum reduction in scoured depth at the toe of the EM, the maximum scoured depth and the scoured length, were found to be approximately 29 – 41%, 29 – 37% and 28 – 34%, respectively, for dense VDLV i.e. the combined arrangement of an EM, and dense VDLV, compared to the percentage difference with OE. The presence of VDLV model behind the EM played a significant role in offering reflection/resistance to the overtopping flow, and thus caused a noteworthy reduction in scoured depth and scoured length, in comparison to that of SLV.
- Maximum energy reduction of flow was found to be approximately 49% – 53% for the dense VDLV. In addition, the formed hydraulic jump behind VM in case of VDLV cases contributed significantly to the total relative energy loss. The loss of relative energy varied due to the combined effect upon the movement of the position of the submerged hydraulic jump toe toward the top of EM, the intensity of the formed hydraulic jump just behind VM and the inundation depth at the downstream of the defense system. Therefore, when a dense VDLV was implemented behind an EM, it gave the maximum dissipation of energy to the flow compared with those of other VM cases.
- With the decrease in porosity and increase in density of short submerged vegetation layer, the position of the submerged hydraulic jump toe (P_j') shifted towards the top of EM. In this study, significant reduction in scouring phenomena was witnessed when the P_j' shifted more towards the top of EM and also resulted more energy loss.

The findings of this paper are important for the ideal design procedures of the defense structures in the coastal regions. This study investigated a fixed width of VM, but if there is abundant space in coastal belt then increasing the width of VM might be a viable option in reducing more scouring within the defense system as it can shift P_j' shifts more towards the EM top by offering increased drag and reflection/resistance to the flow. In this study a non-cohesive gravel particle was used as a soil layer and a constant gap was maintained between the embankment and forest. However, to make the findings of this paper more fruitful, further experimental investigation by changing the gap condition and increasing the width of the VM is needed.

CRediT author statement

Md Abedur Rahman: Conceptualization, Methodology, Model preparation, Investigation, Data processing and analysis, Writing - Original Draft, Visualization.

Norio Tanaka: Conceptualization, Resources, Writing - Review & Editing, Supervision, Project administration, Funding acquisition.

Nijati Reheman: Model preparation, Investigation, Visualization.

Declaration of competing interest

The authors declare that they have no known competing financial interests or personal relationships that could have appeared to influence the work reported in this paper.

Acknowledgements

The authors would like to appreciate the support from the Japanese

Ministry of Education, Culture, Sports, Science, and Technology (Monbukagakusho). Naveed Anjum is acknowledged discussion.

References

Afreen, S., Yagisawa, J., Tanaka, N., 2015. Investigation of scour pattern downstream of levee toe due to overtopping flow. J. Jpn. Soc. Civ. Eng. 71 (4). I_175-I_180, Ser. B1 (Hydraul. Eng.).

Ali, A., Tanaka, N., 2020. Experimental study of scouring downstream of coastal vegetation in an inundating tsunami current. Landsc. Ecol. Eng. 16, 273–287.

Ali, H.M., El-Gendy, M.M., Mirdan, A.M.H., Ali, A.A.M., Abdelhaleem, F.S.F., 2014. Minimizing downstream scour due to submerged hydraulic jump using corrugated aprons. Ain Shams Eng. J. 5, 1059–1069.

Aniel-Quiroga, Í., Vidal, C., Lara, J.L., González, M., Sainz, Á., 2018. Stability of rubble-mound breakwaters under tsunami first impact and overflow based on laboratory experiments. Coast Eng. 135, 39–54.

Anjum, N., Tanaka, N., 2019a. Study on the flow structure around discontinued vertically layered vegetation in an open channel. J. Hydrodyn. 1–14 https://doi.org/10.1007/s42241-019 0040-2.

Anjum, N., Tanaka, N., 2019b. Numerical investigation of velocity distribution of turbulent flow through vertically double-layered vegetation. Water Sci. Eng. 12 (4), 319–329. https://doi.org/10.1016/j.wse.2019.11.001.

Anjum, N., Tanaka, N., 2019c. Experimental study on flow analysis and energy loss around discontinued vertically layered vegetation. Environ. Fluid Mech. 1–27 https://doi.org/10.1007/s10652-019-09723-8.

Bricker, J.D., Francis, M., Nakayama, A., 2012. Scour depths near coastal structures due to the 2011 Tohoku tsunami. J. Hydraul. Res. 50 (6), 637–641. https://doi.org/10.1080/00221686.2012.721015.

Chow, V.T., 1959. Open Channel Hydraulics. McGraw-Hill Publishing Co., New York.

Fadly, U., Murakami, K., 2013. Study on reducing tsunami inundation energy by the modification of topography based on local wisdom. J. Jpn. Soc. Civ. Eng. 68 (I), 66–71.

Foytong, P., Ruangrassamee, A., Shoji, G., Hiraki, Y., Ezura, Y., 2013. Analysis of tsunami flow velocities during the March 2011 Tohoku, Japan, tsunami. Earthq. Spectra 29 (1_Suppl. l), 161–181.

Igarashi, Y., Tanaka, N., 2016. Multiple defense for tsunami inundation by two embankment system and prevention of oscillation by trees on embankment. In: Proceedings of the 20th Congress of IAHR APD Congress, pp. 28–31. Colombo, Sri Lanka.

Iimura, K., Tanaka, N., 2012. Numerical simulation estimating effects of tree density distribution in coastal forest on tsunami mitigation. Ocean. Eng. 54, 223–232.

Japan Society of Fluid Mechanics, 1998. Handbook of Fluid Mechanics, second ed. Japan Society of Fluid Mechanics, Maruzen, Tokyo, pp. 237–240 (in Japanese).

Jayaratne, M.P.R., Premaratne, B., Adewale, A., Mikami, T., Matsuba, S., Shibayama, T., Esteban, M., Nistor, I., 2016. Failure mechanisms and local scour at coastal structures induced by tsunami. Coast Eng. J. 58, 1640017, 04.

Kato, F., Suwa, Y., Watanabe, K., Hatogai, S., 2012. Mechanisms of coastal dike failure induced by the Great East Japan earthquake tsunami. In: Proceeding of 33rd International Conference on Coastal Engineering. Santander, Spain.

Kawagoshi, N., Hager, W.H., 1990. B-jump in sloping channel. J. Hydraul. Res. 28 (4), 461–480.

Lenzi, M.A., Comiti, F., 2003. Local scouring and morphological adjustments in steep channels with check-dam sequences. Geomorphology 55, 97–109.

Matsuba, S., Mikami, T., Jayaratne, R., Shibayama, T., Esteban, M., 2014. Analysis of tsunami behavior and the effect of coastal forest in reducing tsunami force around the coastal dikes. Coast. Eng. Proc. 1 (34), 37.

Mikami, T., Shibayama, T., Esteban, M., 2012. Field survey of the 2011 Tohoku earthquake and tsunami in Miyagi and Fukushima Prefectures. Coast Eng. J. 54 (1), 1–26.

Mitobe, Y., Adityawan, M.B., Tanaka, H., Kawahara, T., Kurosawa, T., Otsushi, K., 2014. Experiments on scouring behind coastal dikes induced by tsunami overflow. J. Jpn. Soc. Civ. Eng. 70. Ser. B1 (Hydraul. Eng.).

Mitobe, Y., Adityawan, M.B., Roh, M., Tanaka, H., Otsushi, K., Kurosawa, T., 2016. Experimental study on embankment reinforcement by steel sheet pile structure against tsunami overflow. Coast Eng. J. 58 (4), 1640018-1.

Nandasena, N.A.K., Sasaki, Y., Tanaka, N., 2012. Modeling field observations of the 2011 Great East Japan tsunami: efficacy of artificial and natural structures on tsunami mitigation. Coast Eng. 67, 1–13.

Noguchi, K., Sato, S., Tanaka, S., 1997. Large-scale model experiment of wave overtopping and frontal surface scouring of revetment due to tsunami run-up. Annu. J. Coast. Eng. 44, 296–300.

Pagliara, S., 2007. Influence of sediment gradation on scour downstream of block ramps. J. Hydraul. Eng. 133, 1241–1248.

Park, H., Cox, D.T., Barbosa, A.R., 2017. Comparison of inundation depth and momentum flux based fragilities for probabilistic tsunami damage assessment and uncertainty analysis. Coast. Eng. 122, 10–26.

Pasha, G.A., Tanaka, N., 2017. Undular hydraulic jump formation and energy loss in a flow through emergent vegetation of varying thickness and density. Ocean Eng. 141, 308–325.

Rahman, M.A., Tanaka, N., Rashedunnabi, A.H.M., Igarashi, Y., 2020. Energy reduction in tsunami through a defense system comprising an embankment and vegetation on a mound. In: Proceedings of the 22nd IAHR-APD Congress. Sapporo, Japan, 6-5-5.

Rashedunnabi, A.H.M., Tanaka, N., 2019. Energy reduction of a tsunami current through a hybrid defense system comprising a sea embankment followed by a coastal forest. Geosciences 9, 247.

Rashedunnabi, A.H.M., Tanaka, N., 2020. Effectiveness of double-layer rigid vegetation in reducing the velocity and fluid force of a tsunami inundation behind the vegetation. Ocean Eng. 201, 107142.

Rashedunnabi, A.H.M., Tanaka, N., Anjum, N., 2019. Effectiveness of hybrid tsunami mitigation system consisting a seaward embankment and a landward horizontally double-layer forest. J. Jpn. Soc. Civ. Eng. 75 (2), 715–720. Ser. B1 (Hydraul. Eng.).

Sassa, S., Takahashi, H., Morikawa, Y., Takano, D., 2016. Effect of overflow and seepage coupling on tsunami-induced instability of caisson breakwaters. Coast Eng. 117, 157–165.

Shuto, N., 1987. The effectiveness and limit of tsunami control forests. Coast. Eng. Jpn. 30 (1), 143–153.

Strusińska-Correia, A., 2017. Tsunami mitigation in Japan after the 2011 Tōhoku tsunami. Int. J. Disaster Risk Reduct. 22, 397–411.

Suppasri, A., Koshimura, S., Imai, K., Mas, E., Gokon, H., Muhari, A., Imamura, F., 2012. Developing tsunami fragility curves from the surveyed data of the 2011 Great East Japan tsunami in Sendai and Ishinomaki Plains. Coast Eng. J. 54 (1), 1250008–1–1250008–16.

Takegawa, N., Sawada, Y., Kawabata, T., 2017. Prediction for scour profile at landward toes of coastal dikes due to tsunami overflow. J. Jpn. Soc. Civ. Eng. Ser. B2 73 (2). I_10451–I_1050.

Takegawa, N., Sawada, Y., Kawabata, T., 2019. Geogrid-based countermeasures against scour behind coastal dikes under tsunami overflow. Mar. Georesour. Geotechnol. 38 (1), 64–72.

Tanaka, N., 2009. Vegetation bioshields for tsunami mitigation: review of the effectiveness, limitations, construction, and sustainable management. Landsc. Ecol. Eng. 5, 71–79.

Tanaka, N., 2012. Effectiveness and limitations of coastal forest in large tsunami: conditions of Japanese pine trees on coastal sand dunes in tsunami caused by Great East Japan Earthquake. J. Jpn. Soc. Civ. Eng. 68 (4) (II_7–II_15). Ser. B1 (Hydraul. Eng.).

Tanaka, N., Sato, M., 2015. Scoured depth and length of pools and ditches generated by overtopping flow from embankments during the 2011 Great East Japan tsunami. Ocean Eng. 109, 72–82.

Tanaka, N., Sasaki, Y., Mowjood, M.I.M., 2006. Effects of sand dune and vegetation in the coastal area of Sri Lanka at the Indian Ocean tsunami. Adv Geosci. Hydro. Sci. 6, 149–159.

Tanaka, N., Sasaki, Y., Mowjood, M.I.M., Jinadasa, K.B.S.N., Homchuen, S., 2007. Coastal vegetation structures and their functions in tsunami protection: experience of the recent Indian Ocean tsunami. Landsc. Ecol. Eng. 3, 33–45.

Tanaka, N., Yagisawa, J., Yasuda, S., 2013. Breaking pattern and critical breaking condition of Japanese pine trees on coastal sand dunes in huge tsunami caused by Great East Japan Earthquake. Nat. Hazards 65, 423–442.

Tanaka, N., Yasuda, S., Iimura, K., Yagisawa, J., 2014. Combined effects of coastal forest and sea embankment on reducing the washout region of houses in the Great East Japan tsunami. J. Hydro-Environ. Res. 8, 270–280.

Tang, X., Rahimi, H., Singh, P., Wei, Z., Wang, Y., Zhao, Y., Lu, Q., 2019. Experimental study of open-channel flow with partial double-layered vegetation. In: E3S Web of Conferences, vol. 81. EDP Sciences, 01010.

Tanimoto, R., Tokida, K., Kitagawa, H., Araki, S., 2012. Investigation on resistance of earth bank and reduction by dug pool against Tsunami. J. Jpn. Soc. Civ. Eng. Ser. B2 68 (2), I_316–I_320. https://doi.org/10.2208/kaigan.68.I_316.

Tappin, D.R., Evans, H.M., Jordan, C.J., Richmond, B., Sugawara, D., Goto, K., 2012. Coastal changes in the Sendai area from the impact of the 2011 Tōhoku-oki tsunami: interpretations of time series satellite images, helicopter-borne video footage and field observations. Sediment. Geol. 282, 151–174.

Thuy, N.B., Nandasena, N.A.K., Dang, V.H., Tanaka, N., 2018. Simplified formulae for designing coastal forest against tsunami run-up: one-dimensional approach. Nat. Hazards 92 (1), 327–346.

Tokida, K., Tanimoto, R., 2014. Lessons for countermeasures using earth structures against tsunami obtained in the 2011 off the Pacific coast of Tohoku earthquake. Soils Found. 54 (4), 523–543.

Vuik, V., Jonkman, S.N., Borsje, B.W., Suzuki, T., 2016. Nature-based flood protection: the efficiency of vegetated foreshores for reducing wave loads on coastal dikes. Coast. Eng. 116, 42–56.

Yanagisawa, H., Koshimura, S., Miyagi, T., Imamura, F., 2010. Tsunami damage reduction performance of a mangrove forest in Banda Aceh, Indonesia inferred from field data and a numerical model. J. Geophys. Res. 115, C06032.

Yoshida, K., Maeno, S., Iiboshi, T., Araki, D., 2018. Estimation of hydrodynamic forces acting on concrete blocks of toe protection works for coastal dikes by tsunami overflows. Appl. Ocean Res. 80, 181–196.

Zaha, T., Tanaka, N., Kimiwada, Y., 2019. Flume experiments on optimal arrangement of hybrid defense system comprising an embankment, moat, and emergent vegetation to mitigate inundating tsunami current. Ocean Eng. 173, 45–57.